Communication

Detection and Mechanistic Relevance of Transient Ligand Radicals Formed during [Ru(bpy)(OH)]O-Catalyzed Water Oxidation

Jonathan L. Cape, and James K. Hurst

J. Am. Chem. Soc., **2008**, 130 (3), 827-829 • DOI: 10.1021/ja077276s

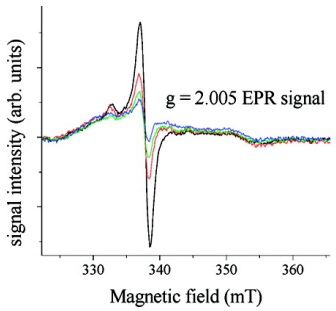

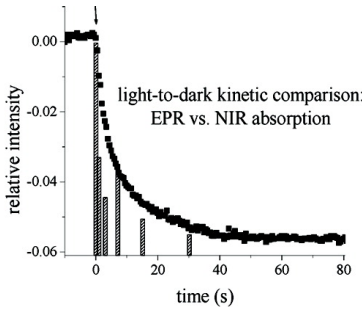

More About This Article

Additional resources and features associated with this article are available within the HTML version:

- Supporting Information
- Access to high resolution figures
- Links to articles and content related to this article
- Copyright permission to reproduce figures and/or text from this article

View the Full Text HTML

J|A|C|S
COMMUNICATIONS

Published on Web 12/28/2007

Detection and Mechanistic Relevance of Transient Ligand Radicals Formed during $[Ru(bpy)_2(OH_2)]_2O^{4+}$-Catalyzed Water Oxidation

Jonathan L. Cape and James K. Hurst*

Department of Chemistry, Washington State University, Pullman, Washington 99164

Received September 24, 2007; E-mail: hurst@wsu.edu

Water oxidation catalyzed by ruthenium diimine complexes of the class $[RuL_2(OH_2)]_2O^{4+}$, where L is 2,2′-bipyridine or a ring-substituted analogue, has been widely studied for over 30 years.[1] This capability makes these complexes attractive for use as catalysts in fuel cells and solar energy photoconversion devices, as well as potentially useful mimics to explore the elusive redox chemistry taking place in multinuclear μ-oxo-bridged metalloenzymes. In acidic media, the catalytically active oxidation state of these complexes is $[RuL_2(O)]_2O^{4+}$, hereafter denoted {5,5},[2] which is reached by net $4e^-$ oxidation of the {3,3} ion accompanied by proton loss from the coordinated aqua ligands. Isotope labeling studies utilizing coordinated $^{18}OH_2$ have identified two major pathways for water oxidation in acidic media, in which either (*a*) one of the O atoms is obtained from the coordination sphere and the other from solvent or (*b*) both O atoms are obtained from solvent.[3,4] Contributions to O_2 formation by pathways involving oxidative coupling of the two terminal oxo atoms are negligible.[1b,3] Pathway *a* has been proposed to involve concerted addition of the elements of H_2O across the $[Ru(O)]_2O$ core of {5,5} to give the peroxy-bound intermediate, $L_2Ru(OOH)-O-Ru(OH)L_2^{4+}$;[1,3] although this intermediate has not been observed, the plausibility of this pathway is supported by ab initio calculations.[5] Pathway *b* is more problematic. Kinetic analyses of isotope evolution rates indicate that water exchange on {5,5} and intermediary oxidation states is very slow relative to O_2 evolution (J. Cape, unpublished observations). We have suggested the following general mechanism for pathway *b* that involves sequential addition of two H_2O molecules to the bipyridine ligands, which ultimately couple to generate O_2:[3]

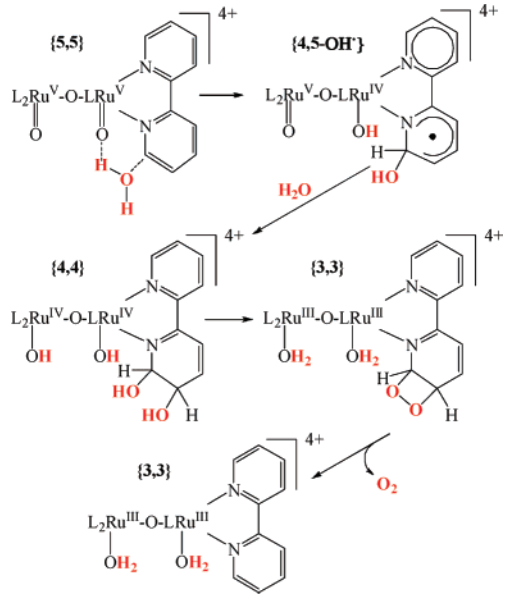

In this scheme, reaction is again initiated by concerted addition of H_2O, but with the OH fragment attaching to the bipyridine ring, analogous to "covalent hydration" reactions of N-heterocyclic compounds.[6] The subsequent steps need not be concerted. By analogy with the reported redox properties of radiolytically generated OH adducts of $Ru(bpy)_3^{2+}$ and free 2,2′-bipyridine,[7] which are moderately strongly reducing, internal electron transfer to the strongly oxidizing Ru−O−Ru core in {4,5-OH•} could generate an intermediary ligand cation, which would be expected to add OH^- in a pseudobase reaction to generate a diol derivative.[7,8] Further internal electron transfer could lead to formation of a dioxetane, which should undergo bond rearrangement with release of O_2.[9]

This mechanism is very similar to those that had been advanced earlier to account for O_2 formation in reactions between $Ru(bpy)_3^{3+}$ and OH^-.[10,11] For both monomeric and dimeric bipyridine complexes, near-infrared (NIR) bands that are diagnostic of bpy-OH adduct formation,[1b,10−12] as well as cryogenic EPR signals attributable to ligand-based radicals,[1c,11] have been reported. Although intermediates of this type are predicted by the proposed mechanisms, the relationships of these transients to various oxidation states of the metal ions have not been clearly identified, nor has their kinetic competence to be bona fide reaction intermediates been demonstrated, for example, as opposed to side products formed by decomposition of the catalysts.[13] In the present study, we have utilized a previously described $S_2O_8^{2-}-RuL_3^{2+}-[RuL_2(OH_2)]_2O^{4+}$ electron acceptor/photosensitizer/catalyst system[14] to probe these relationships; this study was prompted by our recent discovery that steady-state concentration levels of the reaction transients in photocatalytic systems run under neutral conditions are substantially greater than have been observed during chemical catalysis in acid solution.[1c]

Time-resolved absorbance spectra obtained in a typical O_2-evolving photolysis experiment are shown in Figure 1A, where progressive oxidation of {3,3} proceeds via reaction with photogenerated $Ru(bpy)_3^{3+}$. At the redox poise of the system attained in steady state, the solution consists primarily of a mixture of higher oxidation states—{4,4}, {4,5}, and/or {5,5}—that is presently only partially characterized. The {3,4} ion was oxidized at pH 7.2 under constant potential electrolysis (CPE) to a species whose visible absorption band was broader and much less intense than that of {3,4} (Figures 1A and S1, Supporting Information); the midpoint potential (1.1 V vs NHE) matched that obtained by cyclic voltammetry (Figure S1, Supporting Information).[15] Resonance Raman spectra of these solutions gave no indication of bands at ~800 cm^{-1}, which are diagnostic of Ru═O bond formation.[16] In contrast, these bands were readily detected in photolyzed solutions of the dimer (Figures 2 and S3, Supporting Information), indicating that under these conditions further oxidation had occurred to generate a ruthenyl-containing center (either {4,5} or {5,5}). As is the case for {4,4} and {5,5} in acidic media,[16] these oxidation states were virtually indistinguishable by optical spectroscopy (Figure S3,

10.1021/ja077276s CCC: $40.75

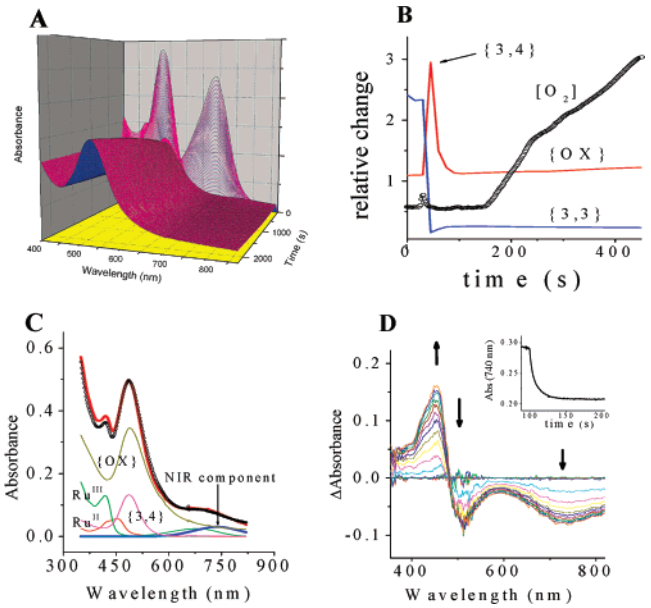

Figure 1. (A) Time-resolved absorbance spectra of photocatalyzed oxidation of 40 μM {3,3} by 60 μM $Ru(bpy)_3^{2+}$ with 5 mM $S_2O_8^{2-}$ in 100 mM phosphate, pH 7.2. (B) Single wavelength traces of the reaction at 636 nm ({3,3}) and 480 nm ({3,4} and {OX} = {4,4} + {4,5} +{5,5}); the open circles are simultaneously measured O_2 concentrations. The data indicate an initial conversion of {3,3} to {3,4} characterized by a bleaching at 636 nm and an increase in absorbance at 480 nm, followed by conversion of {3,4} to a mixture of the higher redox states. (C) Least-squares component fitting of the steady-state spectrum assuming contributions from {3,3}, {3,4}, the higher redox states (denoted as {OX}), the photosensitizer (Ru^{II} and Ru^{III}), and an assumed Gaussian-shaped NIR absorption band. (D) Difference spectra following an abrupt dark transition from steady state and kinetics at 740 nm (inset) showing decay of the NIR intermediate.

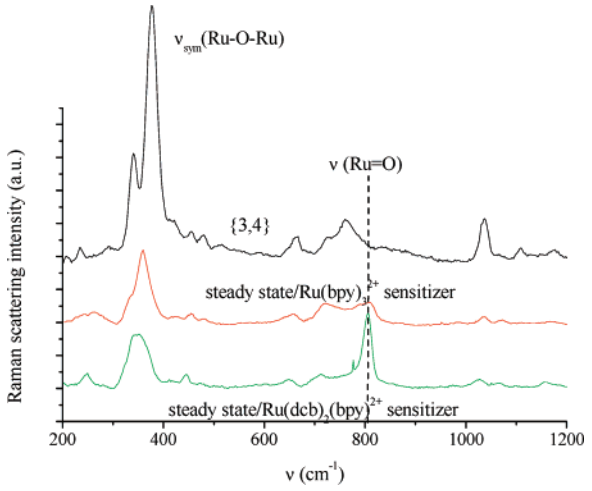

Figure 2. Low-frequency resonance Raman spectra (λ_{ex} = 496.5 nm) of 0.1 M phosphate solutions, pH 7.2, containing 150 μM dimer and 5 mM $S_2O_8^{2-}$. Red trace: steady-state spectrum under continuous illumination in the presence of 100 μM $Ru(bpy)_3^{2+}$. Green trace: same conditions, except with $Ru(dcb)_2(bpy)^{2+}$ as photosensitizer. The black spectrum is that of {3,4} generated by dark oxidation of {3,3} by $S_2O_8^{2-}$. The Ru=O stretching frequency appears at 806 cm^{-1}, similar to the value of 818 cm^{-1} previously reported for {5,5}.[16] Other prominent features are the intense redox state-dependent Ru−O−Ru symmetric stretching bands appearing at 344−386 cm^{-1} and their first overtones at 2 × υ_{sym}(Ru−O−Ru). The relatively broad band at centered at 344 cm^{-1} in the lowest trace indicates that complete steady-state conversion to the higher oxidation state has not been achieved in this strongly photooxidizing system.

Supporting Information). Simultaneous measurement of O_2 generation using a Clark-type microelectrode immersed in the reaction medium indicated that O_2 evolution occurs only after the higher oxidation states have accumulated (Figure 1B). The steady-state optical spectra obtained under continuous illumination were fit as described in Supporting Information as linear combinations of identifiable species using authentic spectra of {3,3}, {3,4}, the CPE-generated intermediate, $Ru(bpy)_3^{2+}$, and $Ru(bpy)_3^{3+}$. (Since the two accumulating higher oxidation states of the dimer have nearly identical spectra, the experimental fit represents the sum of these species.) Adequate fits could only be achieved by introducing an additional NIR-absorbing species with $\lambda_{max} \sim 740$ nm and $\epsilon = 1000\ M^{-1}\ cm^{-1}$ (Figure 1C). This species was observed only when O_2 was simultaneously being produced in the reaction and was not observed in spectra of the oxidized ion produced by controlled potential electrolysis. Its spectral properties are very similar to those of the $M(bpy)_2(bpy\text{-}OH)^{n+}$ adducts,[10,12] as well as transients formed in the reaction of radiolytically generated $OH^{\bullet}$ with {3,3} and {3,4}.[1b]

Kinetic measurements were made to verify that the NIR band was not an artifact of the spectral fitting procedure (Figure 1D). A steady-state concentration of reaction transients was generated by continuous photolysis with a 470 nm LED bank, and spectral changes occurring upon turning off the light were recorded using a diode array spectrophotometer. Three decay features appeared in the dark interval difference spectra (Figure 1D), which can be assigned as decay of the NIR band at 740 nm, small absorbance changes associated with interconversion of higher oxidation states at ~510 nm, and an increase in $Ru(bpy)_3^{2+}$ absorbance at 450 nm. The rate constants for decay at 510 and 740 nm were identical ($\tau \sim 5$ s), suggesting that they arose from either the same or rapidly equilibrating species.

Use of the more strongly oxidizing sensitizer $(Ru(dcb)_2(bpy)^{2+}$, dcb ≡ 4,4′-dicarbethoxy-2,2-bipyridine; $E^o(Ru^{III/II}) = 1.51$ V (NHE)) caused the photocatalyzed rate of O_2 formation to increase ~5-fold over that when $Ru(bpy)_3^{2+}$ ($E^o(Ru^{III/II}) = 1.27$ V) was the sensitizer under otherwise identical conditions. The steady-state level of the ruthenyl-containing transient increased proportionately (Figure 2), strongly implying that the more highly oxidized complex is the oxygen-evolving state.

Several lines of evidence, summarized below, indicate that the NIR band derives from the μ-oxo dimer and not the photosensitizer: (1) the amplitude of the NIR signal was proportional to the concentration of the μ-oxo catalyst but was independent of the sensitizer concentration. (2) The λ_{max} at 740 nm and relatively large amplitude and decay rate distinguish it from a 680 nm band ($\epsilon_{680} \sim 300\ M^{-1}\ cm^{-1}$) associated with $Ru(bpy)_3^{3+}$, which undergoes recovery to $Ru(bpy)_3^{2+}$ at a slower rate ($\tau \sim 30$ s, measured at 450 nm (Figure 1D)). Likewise, the optical properties of the NIR band are different from those reported[10] for the pseudobase intermediate formed via reductive addition of OH^- to the bipyridine ligand of $Ru(bpy)_3^{3+}$ ($\lambda_{max} = 800$ nm). This intermediate could not be detected in photolyzed samples containing just $Ru(bpy)_3^{2+}$and $S_2O_8^{2-}$. (3) Functional group substitution on the bipyridine ligands of the μ-oxo dimer altered the properties of the accumulating NIR transients, with λ_{max}= 735 and 758 nm for 4,4′-dimethyl and 4,4′-dicarboxy analogues, respectively (Figure S8, Supporting Information), and relative rate constants for NIR decay decreasing in the order 4,4′-dimethylbpy > bpy > 4,4′-dicarboxybpy. Relaxation times measured at pH 7.2 were τ ~6, ~9, and ~37 s, respectively.

A relatively narrow $g = 2.005$ signal was observed in the 77 K EPR spectra of rapid freeze-quenched samples (Figure 3A) that is similar to signals appearing in acidic solutions of chemically or electrochemically generated {5,5}; the latter have been provisionally assigned as ligand-centered radicals.[1c] Power saturation studies (Figure S6, Supporting Information) indicated that the photochemi-

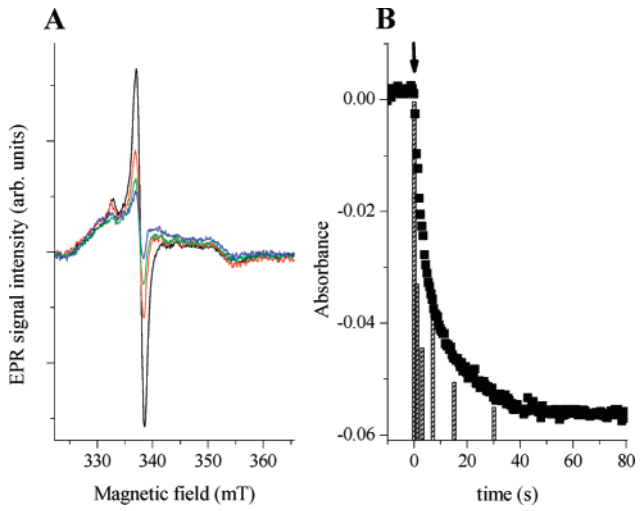

Figure 3. EPR spectra and dark transition decay kinetics of the $g = 2.005$ radical signal produced during photocatalytic O_2 evolution. (A) Signal intensity at 0, 1, 3, and 15 s after a light-to-dark transition. (B) Comparison of the time-resolved signal amplitude (shaded bars) with the decay of the $\lambda = 740$ nm absorbance signal (closed squares). The arrow indicates the point at which illumination was blocked.

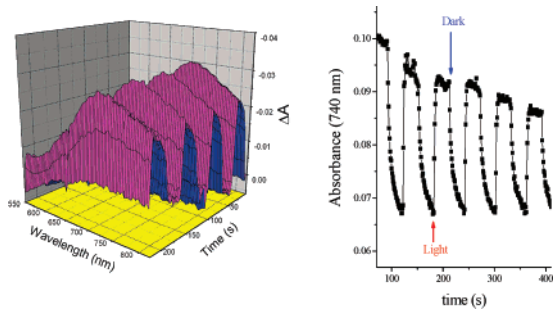

Figure 4. Reversible formation of the ligand radical band upon light/dark cycling. On the right is shown the single wavelength trace at 740 nm; the red and blue arrows indicate the point at which illumination at 470 nm starts and stops, respectively. The decrease in maximal amplitude under repetitive cycling is due to depletion of $S_2O_8^{2-}$.

cally generated radical is in close proximity to a fast relaxing metal center, with a half saturation point (>10 mW) substantially higher than that commonly observed for organic radicals (<100 μW). The rate constant determined for decay of the $g = 2.005$ signal ($\tau \sim 7$ s) was nearly identical to the NIR absorbance decay (Figure 3B), suggesting that they are either properties of a single transient or species that are in rapid equilibrium with each other.

Upon blocking the light from the illumination source, the NIR-absorbing transient decayed with the same rate constant as cessation of O_2 evolution (e.g., $\tau \sim 50$ s vs $\tau \sim 66$ s at pH 3.5), and the rate constant for NIR decay was proportional to the steady-state rate constant for O_2 evolution over the entire pH range investigated (i.e., pH 2−10, Figure S7, Supporting Information). The NIR-absorbing transient could be formed reversibly upon cycling between the O_2-evolving and lower redox states of the catalyst by applying alternating intervals of illumination and darkness (Figure 4). This observation provides further evidence that the transient concentration tracks with the amount of active catalyst and therefore meets minimal requirements for kinetic competency as a reaction intermediate.

We suggest that covalent hydration[6] from the {5,5} state produces a transient {4,5}-bpy(OH) radical intermediate that is responsible for the NIR absorbance and EPR signal.[3] Decay of this species may involve additional covalent hydration[6b] or pseudobase formation[8] to produce a {4,4}-bpy$(OH)_2$ diol, which undergoes further reaction in the catalytic cycle to generate O_2. Ongoing work is directed at structurally characterizing the NIR-absorbing and EPR-active transients.

Acknowledgment. The authors are grateful to Jeanne McHale for providing access to her Raman facility at WSU, and to Jonathan A. Downing for assistance in making the resonance Raman measurements. This research is supported by the Office of Basic Energy Sciences, U.S. Department of Energy (Grant DE-FG02-06ER15820).

Supporting Information Available: Figures S1−S8 and a summary of methods used in component fitting of the steady-state optical spectra. This material is available free of charge via the Internet at http://pubs.acs.org.

References

(1) (a) Liu, F.; Concepcion, J. J.; Cardolaccia, T.; Jurss, J. W.; Meyer, T. J. *Inorg. Chem.* **2007**, *46*, in press. (b) Hurst, J. K.; Cape, J. L.; Clark, A. E.; Das, S.; Qin, C. *Inorg. Chem.* **2007**, *46*, in press. (c) Hurst, J. K. *Coord. Chem. Rev.* **2005**, *249*, 313−328.
(2) This notation indicates only the formal oxidation state of the metal ions. The extent of electron delocalization within the complex is unresolved and under active investigation.[1a,b]
(3) Yamada, H.; Siems, W. F.; Koike, T.; Hurst, J. K. *J. Am. Chem. Soc.* **2004**, *126*, 9786−9795.
(4) Geselowitz, D. A.; Meyer, T. J. *Inorg. Chem.* **1990**, *29*, 3894−3896.
(5) Yang, X.; Baik, M.-H. *J. Am. Chem. Soc.* **2006**, *128*, 7476−7485.
(6) (a) Albert, A.; Armarego, W. L. F. *Adv. Heterocycl. Chem.* **1965**, *4*, 1−42. (b) Albert, A. *Adv. Heterocycl. Chem.* **1976**, *20*, 117−143.
(7) Maliyackel, A. C.; Waltz, W. L.; Lilie, J.; Woods, R. J. *Inorg. Chem.* **1990**, *29*, 340−348.
(8) Bunting, J. W. *Adv. Heterocycl. Chem.* **1979**, *25*, 1−82.
(9) Wasserman, H. H.; Scheffer, J. R. *J. Am. Chem. Soc.* **1967**, *89*, 3073−3075.
(10) Creutz, C.; Sutin, N. *Proc. Natl. Acad. Sci. U.S.A.* **1975**, *72*, 2858−2862.
(11) Ledney, M.; Dutta, P. K. *J. Am. Chem. Soc.* **1995**, *117*, 7687−7695.
(12) (a) Dimitrijević, N. M.; Mićić, O. I. *J. Chem. Soc., Dalton Trans.* **1982**, 1953−1957. (b) Mulazzani, Q. G.; Venturi, M.; Bolletta, F.; Balzani, V. *Inorg. Chim. Acta* **1986**, *113*, L1−L2.
(13) Ghosh, P. K.; Brunschwig, B. S.; Chou, M.; Creutz, C.; Sutin, N. *J. Am. Chem. Soc.* **1984**, *106*, 4772−4783.
(14) (a) Rotzinger, F. P.; Munavalli, S.; Comte, P.; Hurst, J. K.; Grätzel, M.; Frank, A. J. *J. Am. Chem. Soc.* **1987**, *109*, 6619−6626. (b) Comte, P.; Nazeerudin, M. K.; Rotzinger, F. P.; Frank, A. J.; Grätzel, M. *J. Mol. Catal.* **1989**, *52*, 63−84.
(15) (a) Gilbert, J. A.; Eggleston, D. S.; Murphy, W. R., Jr.; Geselowitz, D. A.; Gersten, S. W.; Hodgson, D. J.; Meyer, T. J. *J. Am. Chem. Soc.* **1985**, *107*, 3855−3864. (b) Gilbert, J. A.; Geselowitz, D.; Meyer, T. J. *J. Am. Chem. Soc.* **1986**, *108*, 1493−1501.
(16) Yamada, H.; Hurst, J. K. *J. Am. Chem. Soc.* **2000**, *122*, 5303−5311.

JA077276S